PCCP

Accepted Manuscript

ROYAL SOCIETY OF CHEMISTRY

www.rsc.org/pccp

Physical Chemistry Chemical Physics
CREATED USING THE RSC LaTeX PCCP ARTICLE TEMPLATE – SEE www.rsc.org/electronicfiles FOR DETAILS
ARTICLE TYPE www. rsc.org/xxxxxx | XXXXXXXX

Role of shape resonance state during low energy electron induced single strand break in 2′-deoxycytidine-5′-monophosphate†

Renjith Bhaskaran and Manabendra Sarma*

Received Xth XXXXXXXXXX 20XX, Accepted Xth XXXXXXXXX 20XX
First published on the web Xth XXXXXXXXXX 20XX
DOI: 10.1039/b000000x

Low energy electron (LEE) induced single strand break (SSB) has been studied for 2′-deoxycytidine-5′-monophosphate (5′-dCMPH) molecule in gas phase by means of ab-initio electronic structure methods and local complex potential based time-dependent wavepacket quantum mechanical calculations. We have found that the LEE attachment to this cytidine nucleotide results in the formation of a transient metastable anion. The results obtained show that the electron attachment takes place at the cytosine nucleobase center and within 18–20 fs, the LEE transfers to the σ^* orbital of the sugar-phosphate 5′ C–O bond. The characteristic electron attachment cross section spectrum is found $\sim$ 1 eV, which is in good agreement with the available experimental observations. Quantum mechanical tunneling of the 5′ C–O bound vibrational energy levels may contribute to SSB only above 1.5 eV energy regimes.

1 Introduction

Low energy electron (LEE) mediated reduction of bio-molecules gives rise to numerous chemical modifications which abruptly affects the function of cell processes.[1,2] Some of these irreversible changes includes damage to amino acids, DNA strand break, peptide bond cleavage, and so forth.[1–3] Among these damages, DNA single strand breaks (SSBs) receives considerable attention due to the specific site selectivity of the very low energy electron (0–3 eV) binds with the system.[4,5] Recent progresses in these fields reveals that the electron can attach to DNA/DNA fragments in any one of the components like (i) nucleobase,[6] (ii) sugar,[7] (iii) phosphate group[8] or, as a dipole bound state (DBS)[9] outside the molecular framework.[2] The LEE attachment to the target may lead to either the formation of a metastable state [also known as temporary negative ion (TNI)] or an electronically stable anionic species. Metastable state, usually lies above it's parent neutral state (negative electron affinity) are often referred to as "resonance" and exist only for a very short period of time. The TNI plays a prominent role during LEE induced damage to bio-molecules like DNA, causing mutagenesis to the organisms.[1,10] Hence, a large number of secondary electrons which are produced as a result of the interaction of primary ionizing radiation with living cells[11,12] offers a critical threat to the metabolic activities.[10]

In general, a metastable state ($AB^{-\#}$) formed from electron (energy below the ionization potential of the molecule) attachment to a neutral molecule (AB) in an initial state $AB(v_i)$, can relax either through auto-detachment to the target in some excited state [$AB(v_f)$] (Eq. 1) or via fragmented to generate radical(s) and anion(s) [Eq. 2] as

$$AB(v_i) + e^- \rightarrow AB^{-\#} \rightarrow AB(v_f) + e^- \quad (1)$$

$$AB(v_i) + e^- \rightarrow AB^{-\#} \rightarrow A^{\bullet} + B^- \quad (2)$$

The "resonance state" ($AB^{-\#}$) act as a reactive intermediate for a number of electron induced processes and is very difficult to characterize such short lived species using the available experimental techniques.[2] On the other hand, advanced theoretical methods can take into account of the metastability of such intermediate state to a desirable degree of accuracy.[2] The formation and subsequent decay of the TNI is found to be the common mechanistic pathway during dissociative electron attachment (DEA) to DNA/DNA fragments.[13] Therefore, understanding the features of the TNI is an essential step for formulating new strategies in cellular radiolysis and for the design of radiosensitizing drugs for an effective measure for cancer therapy,[10] since the action of LEE is selective to some particular chemical bond within the system.[5]

1.1 Previous Studies

The article published by Sanche and co-workers in *Science* magazine triggered a breakthrough in the area of LEE induced

† Electronic Supplementary Information (ESI) available: [The optimized structures of neutral and anionic 5′-dCMPH moieties using the ab initio HF and MP2 methods, the time evolution plots of ground state eigenfunction of HF potential, the "S-shaped" transmission coefficient values of 5′ C–O bond tunneling from HF and MP2 anionic potentials, the wave packet propagation of twelfth excited state eigenfunction of HF potential, and the SOMOs showing electron transfer during single strand breaks.]. See DOI: 10.1039/b000000x/

* Department of Chemistry, Indian Institute of Technology Guwahati, Guwahati, India. Fax: +91 361 258 2349; Tel: +91 361 258 2318; E-mail: msarma@iitg.ernet.in

DNA damage investigations.[4] Since then, a number of studies have been reported in the literature and are going on in this emerging field.[2,3] Crossed electron-molecular beam experiment upon gas phase 2′-deoxycytidine-5′-monophosphate (5′-dCMP) molecule (without neutralization)[14] concludes that (a) LEE can attach to either the nucleobase cytosine, sugar unit, or the phosphate group, and (b) the contribution towards SSBs varies with respect to each of these sites where the LEE gets attached. A near 0 eV electron can attach to the backbone phosphate group results in *ca.* 60% of the strand breaks, while a near 1 eV LEE can induce SSB (*ca.* 15%) after gets attached to the cytosine nucleobase. The remaining 25% damage is due to the electron initially localized at the ribose sugar unit. The study remarked the formation of entire phosphate ion (PO_4^-) due to two overlapping resonances peaking near 0 eV and 1 eV.[14] On the contrary, theoretical investigation of Bao et al. on modeled 5′-dCMPH moiety (where one of the generated radical center is terminated with methyl group) in both gas phase and aqueous medium suggested the plausibility of a near 0 eV electron attachment exclusively at the nucleobase region.[15] In addition, they also pointed out that the rate of SSB in gas phase is more, compared to that of in aqueous environment.[15] Owing to the discrepancy found in the theoretical and the recent experimental findings, here we present the results obtained from our local complex potential based time dependent wave packet (LCP-TDWP) calculations for this molecule in detail. Along these lines, we have already modeled the 3′ C–O and glycosidic N–C bond dissociation channels in 3′-dCMPH molecule using the LCP-TDWP approach.[16–19] We have noted the following points from our time-dependent wavepacket calculations:

(a) The low energy electron attachment takes place at the cytosine nucleobase center in the low energy 0.5–1 eV region.
(b) The LEE can effectively transfer to the backbone phosphate center via atomic orbital overlap.
(c) It is the 3′ C–O bond which is going to be dissociated in comparison with the glucosidic N–C bond lesion.
(d) The metastable species formed possess a lifetime of around 10–18 fs which can undergo uni-molecular dissociation in competition with the autodetachment process.

Our objective in this paper is to look into the possible LEE attachment sites within this building block (5′-dCMPH) of life and deduce the characteristic fragmentation profiles which may help to understand *the role of shape resonance states* during LEE induced SSB. It has been reported recently from a DFT calculation[20] using the hybrid functionals that the C–O bond cleavage [either the 3′ C–O or the 5′ C–O] in cytidine nucleotide is quite difficult as compared with the previous investigations[15]. A good choice of dispersion corrected functional is therefore essential to model the dissociative electron attachment reactions in molecules. Owing to these discrepancies to assess the *role of shape resonance state* involved during the DNA strand break, one needs to reconsider the choice of correct ab initio method. Although quite cost effective, from our previous efforts[16–19] we consider second-order Møller Plesset perturbation (MP2) method is a better choice in this regard. Moreover, no MP2 calculations have been done within this molecule although it overestimates the dispersion energy. A short description of the electronic structure calculations and the wave packet propagation scheme is mentioned in Section 2. Section 3 narrates the prominent results obtained and the role of shape resonance state during LEE induced SSB. The major outcome from this investigation concludes the paper.

2 Methodology

2.1 Molecular Modeling

Before explaining the details of the time dependent quantum mechanical aspects, let us briefly discuss about the modeled gas phase system 2′-deoxycytidine-5′-monophosphate, in short 5′-dCMPH for LEE induced SSB considered in the present investigation (Fig. 1). The molecular model of the nucleotide used is excised from a portion of double stranded DNA contains the pyrimidine base cytosine, the ribose sugar, and the phosphate group. This fragment possesses the LEE attachment sites and the site where the strand breaks occur. Usually, electro-neutrality in *in vivo* DNA is offered by the presence of group I alkali metal counter cations like Na^+ or K^+ to the negative center of the phosphate group. However, we have chosen two hydrogens and a proton to neutralize the modeled system for relatively smooth attachment of the incoming low energy electron. Such a model will not affect much in terms of the energy region where the incoming electron attaches.

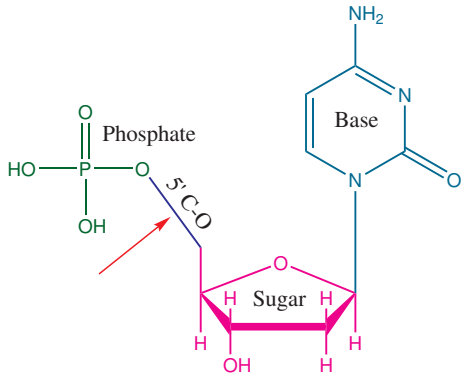

Fig. 1 The modeled 2′-deoxycytidine-5′-monophosphate (5′-dCMPH) molecule neutralized by adding hydrogens at the radical center and a proton at the phosphate negative center. The bond undergoing lesion is marked with a red arrow.

2.2 Geometry Optimization and Potential Energy Scan

The neutral and anionic systems were optimized initially at the Hartree-Fock (HF) and later at the correlated second-order Møller Plesset perturbation theory (MP2) methods at the 6-31+G(d) accuracy level. This is in accordance with our earlier investigation for LEE induced SSB and N–C bond fragmentation within a similar moiety.[16–19]

The optimized geometries were used to compute the potential energy (PE) curves for the target [E_A(R)] and anionic [E_{A^-}(R)] systems (where A = 5′-dCMPH), those are the necessary ingredients for our wave packet propagation calculations. The labeled 5′ C–O bond of Fig. 1 has been compressed/stretched within the interval of 1-10 a_0 for 256 equally spaced grid points for both the neutral and anionic systems, keeping all other degrees of freedom of the molecule frozen. GAUSSIAN 09 package of programs[21] have been used in all of the electronic structure calculations presented here. It has to be noted here that we have not included the rotational levels for the dynamical calculations since this motion normally happens in the longer timescale compared to the vibrational motion.

2.3 Quantum Dynamical Calculation

The local complex potential (LCP) formalism for describing the dynamics of the nuclei of a metastable anion is explained below. Since, it is computationally very difficult to consider the quantum multi-dimensional analysis of relevant biological molecular network, we have considered the one-dimensional 5′ C–O bond dissociation channel in the gas phase 5′-dCMPH molecule (Fig. 1). Anionic species is obtained by adding an electron to the lowest unoccupied molecular orbital (LUMO) of the neutral molecule (A), which in the present context known as TNI [A^-]. This temporary species possess a typical lifetime of around 10-100 fs.[5] The anionic Hamiltonian for the 5′ C–O bond dissociation in LCP-TDWP method is expressed in terms of the kinetic (using the reduced mass of the C–O bond, μ_{A^-}) and LCP energies as

$$H_{A^-}(R) = -\frac{\hbar^2}{2\mu_{A^-}}\nabla^2 + W_{A^-}(R) \tag{3}$$

where, $W_{A^-}(R) = E_{A^-}(R) - \frac{i}{2}\Gamma_{A^-}(R)$ is called the local complex potential[22,23] coined by two necessary ingredients for our time dependent quantum mechanical calculations. The first term is the PEs of the anion [$E_{A^-}(R)$] which is obtained using G09 program suite[21] as discussed in the section 2.1 and the other unknown quantity $\Gamma_{A^-}(R)$ is computed as an exponential function, $\Gamma_{A^-}(R) = \delta_1 \times exp(-\alpha R)$. The $\Gamma_{A^-}(R)$ in the electron molecule scattering theory is termed as "the width function" and is related to the life-time (τ) of the resonance as $\tau = \frac{\hbar}{\Gamma_{A^-}}$. The width function becomes close to zero at the crossing point (R = R_x) between $E_A(R)$ and $E_{A^-}(R)$, thereby ensures the metastability associated with the TNI (A^-).

The metastable state in the LCP-TDWP formulation can be represented using

$$\psi_i(R,t) \simeq U_{A^-}(t)\phi_i(R) \tag{4}$$

where $U_{A^-}(t) = e^{-iH_{A^-}(R)t/\hbar}$ is the evolution operator. The first step of our molecular quantum dynamical calculation is the computation of the grid representation of the wave function of the neutral (A) [ϕ_i(R)] and anionic (A^-) [χ_i(R)] systems at time t = 0, utilizing the extremely efficient Fourier grid Hamiltonian method.[24] The initial wave packet prepared so is then propagated for a finite time limit in space employing the iterative Lanczos based diagonalization scheme[25] to find out the final quantum state distribution. The time dependent Schrödinger equation, which is the pillar for any gas phase and condensed phase quantum dynamical calculations have been used for solving the wave packet propagation sequence

$$i\hbar\frac{\partial\psi_i}{\partial t} = \hat{H}_{A^-}\psi_i \tag{5}$$

in which the performance of the fast Fourier transform (FFT)[26] technique to determine the effect of kinetic energy operator in the anionic Hamiltonian $H_{A^-}(R)$ is well appreciated. Fourier transformation of the auto correlation function [$\langle\chi_i(R)|\psi_i(R,t)\rangle$] gives the fragmentation profile [σ(E)] which is one of the prime objective of our investigation and is calculated using the following relation[27]

$$\sigma(E) = \int_{-\infty}^{\infty} exp(iEt/\hbar)\langle\chi_i(R)|\psi_i(R,t)\rangle dt \tag{6}$$

and compared with the available experimental cross-section spectra.

Finally, there may be a possibility of coupling between the valence π^* shape resonance state and the repulsive σ^* state within the system which may influence as an avoided crossing of the 5′ C–O bond and give rise to a hyperbolic cosine barrier in the anionic PE curve. This will allow the 5′ C–O bound vibrational levels to tunnel toward the repulsive region through the barrier. The transmission coefficient, T, under this circumstance can be computed using any one of the following equations:[28,29]

$$T = \frac{\sinh^2(\pi k/a)}{\sinh^2(\pi k/a) + cos^2[\frac{1}{2}\pi\sqrt{1-K}]} \quad \text{for } K < 1 \tag{7}$$

or,

$$T = \frac{\sinh^2(\pi k/a)}{\sinh^2(\pi k/a) + cosh^2[\frac{1}{2}\pi\sqrt{K-1}]} \quad \text{for } K > 1 \tag{8}$$

where we have defined the constant $K = 8mU_0/\hbar^2a^2$ with U_0 is the height of the potential barrier, and the inverse of full width at the half maximum (FWHM) of the anionic PE curve as "a", the width parameter. The other constant k is calculated as $\frac{(2mE_i)^{\frac{1}{2}}}{\hbar}$ where m is taken as the reduced mass of the 5′ C–O bond and E_i as the energy of the bound vibrational state (i) of $E_{A^-}(R)$.

3 Results and Discussions

3.1 Optimized Geometries and PE curves

The HF and MP2 optimized structures of neutral and anionic systems are provided in Figs. S1(A) and S1(B)†of the supporting information. The equilibrium neutral 5′ C–O bond [R_{C-O} = 2.703 a_0 (1.430 Å) at HF and 2.754 a_0 (1.457 Å) at MP2] is found to be shortened than that of the anion [R_{C-O} = 2.718 a_0 (1.438 Å) at HF and 2.767 a_0 (1.464 Å) at MP2] in both the ab-initio methods. The PE curves calculated for neutral [$E_A(R)$] and anionic [$E_{A^-}(R)$] 5′-dCMPH moieties from the optimized structures (Fig. S1) using G09 codes[21] at the HF and MP2 methods with 6-31+G(d) accuracy levels are shown in Figs. 2(a) and 2(b) respectively. It is clear from these figures that the anion formed is metastable (vertical attachment energy (VAE) is 0.59 eV at HF and 0.35 eV at MP2) at both these methods. Careful inspection of the anionic PE curves enable us to infer that the barrier position in HF [$R_{C-O} \sim 3.84$ a_0 (2.03 Å)] and MP2 methods [$R_{C-O} \sim 3.78$ a_0 (1.99 Å)] are almost similar, though the barrier height differs as 2.14 eV in the former and 1.70 eV in the latter methods respectively.

Since, both HF and MP2 methods results show similar characteristics especially the formation of metastable anionic state after the LEE attachment, therefore, we focus on the results of time dependent quantum mechanical calculations carried out for correlated MP2 potentials. We have also noted that our MP2/6-31+G(d) optimization of the neutral 5′-dCMPH molecule generate the lowest unoccupied molecular orbital approximately at 0.9 eV, showing the π^* antibonding character on the cytosine base moiety. This energy is close to the already reported electron attachment energy regions in cytosine fragments[5] and therefore, we have carried out our time dependent wave packet dynamics to investigate the unimolecular bond dissociation process at a molecular level. HF based results will be stated wherever it is necessary.

3.2 Time-dependent Calculations

The crossing point (R_x) between the neutral and anionic PE curve in MP2 method is 3.83 a_0 (2.02 Å) [3.94 a_0 (2.08 Å) in HF method]. Time dependent calculations have been done on a curtailed slice of $E_A(R)$ and $E_{A^-}(R)$ ranging from R_{C-O} = 1.88 – 4.12 a_0 with 256 equally discretized points in both the *ab initio* methods. The width function [$\Gamma_{A^-}(R)$] is calculated at each grid points for MP2 potential by choosing an optimal values of α = 3.61 and δ_1 = 490 (α = 3.50 and δ_1 = 370 for HF potential) which ensures the metastability of the short lived resonance intermediate state. A plot of $\Gamma_{A^-}(R)$ at each grid points with respect to the 5′ C–O bond distance (R_{C-O}) is shown in Figs. 2(c) and 2(d) for HF and MP2 potentials respectively. The width function goes to nearly zero at the crossing point (R_x) as mentioned in section 2.2.

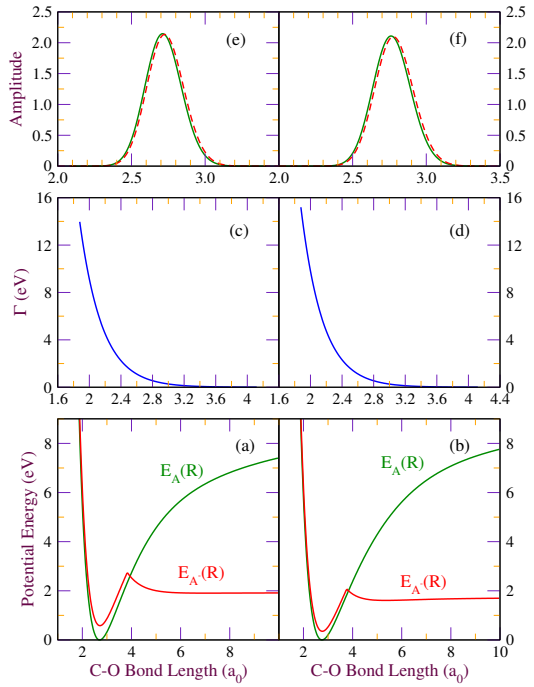

Fig. 2 Potential energy curves for the neutral [$E_A(R)$] (green solid line) and the anionic [$E_{A^-}(R)$] (red solid line) 5′-dCMPH molecule computed at the (a) HF/6-31+G(d), and (b) MP2/6-31+G(d) accuracy level. The width function $\Gamma_{A^-}(R)$ calculated as an exponential function for (c) HF, and (d) MP2 potentials of 5′-dCMPH moiety. The ground state eigenfuntion are shown in (e) for HF [green solid line for neutral and red dashed line for anion], and (f) for MP2 [green solid line for neutral and red dashed line for anion] potentials respectively.

We have, then, computed the vibrational eigenfunctions of the neutral [$\phi_i(R)$] and anionic [$\chi_i(R)$] systems to get the dynamical aspects of LEE induced single strand breaks in 5′-dCMPH moiety. Implementation of the FGH method[24] on the anionic PE curve [$E_{A^-}(R)$] revealed fifteen bound vibrational states for MP2 potential and eighteen bound vibrational levels for HF potential. The ground vibrational levels of both the neutral and anionic systems are shown in Figs. 2(e) and 2(f) respectively for HF and MP2 potentials. It is to be noted here that the anionic wave functions are slightly move forward to the right turning point of the PE curve.

The hyperbolic cosine barrier seen in $E_{A^-}(R)$ for both the HF and MP2 methods may be resulted as the coupling between the valence π^* shape resonance state and the repulsive σ^* state within the system, thereby allowing the 5′ C–O bond to follow an avoided crossing pathway. Consequently, the probability of 5′ C–O bond tunneling from the higher anionic bound vibrational levels through this barrier towards the repulsive region may be very high. Therefore, we have divided the vibrational energy levels [$\chi_i(R)$] of MP2 anionic potential into two regions, those with energy (i) below 1.5 eV [$\chi_{i=0-9}(R)$] and (b) above 1.5 eV [$\chi_{i=10-14}(R)$]. Similarly for HF anionic potential with energy (i) below 1.5 eV [$\chi_{i=0-10}(R)$] and (b) above 1.5 eV [$\chi_{i=11-17}(R)$]. This classification will enable us to focus on the effect of quantum tunneling during LEE induced SSB in 5′-dCMPH molecule which, to the best of our knowledge, has not appeared in the literature yet.

3.2.1 SSB from the ground vibrational level [ϕ_0(R)]. Quantitative treatment of LCP-TDWP approach comprises of three steps in which in the first step, wave packet propagation of the initial bound vibrational state (ϕ_0 in the present context) has been carried out from time t = 0 – 198 fs under the effect of the metastable anionic Hamiltonian [$H_{A^-}(R)$]. Fig. 3 depicts a few plots of this quantum state evolution for MP2 potential (see Fig. S2†for HF potential) at t = 0 – 22 fs in the interval of 2 fs where we can see (i) the progress of the metastable state with maximum amplitude when propagation starts, and goes to negligible values by t = 20 fs with the amplitude being reduced to $4x10^{-6}$ and (ii) the movement of the wave function towards the right turning point of the anionic PE curve characterizing the *impulse model* resonance in e-DNA scattering. This is further ensured from the life time of the metastable anion (18 – 20 fs) which is less than what is required for a C–O bond single vibration ($\sim$ 33 fs). Similar trend can be seen in HF results (see Fig. S2†).

We further proceed to the second step of the quantitative analysis where we have analyzed the auto correlation function $\langle\chi_0(R)|\psi_0(R,t)\rangle$ [Fig. 4(a)] which clearly exhibits the maximum overlap during the initial time of propagation and nullifies near about t = 15 – 20 fs. The fragmentation profile [$\sigma_{0\leftarrow0}(E)$] is computed from the Fourier transformation of the auto correlation function in the final step and is compared with the experimental results[14] of gas phase 5′-dCMP molecule investigation (shoulder near 1 eV) as shown in Fig. 4(b). The calculated $\sigma_{0\leftarrow0}(E)$ spectrum from this investigation is in accordance with the experimental profile[14]. The maximum in the fragmentation profile [$\sigma^{max}_{0\leftarrow0}(E)$] for our time-dependent wavepacket calculation is seen at 0.44 eV for MP2 potential [magenta solid line of Fig. 4(b)] and at 0.67 eV [blue solid line of Fig. 4(b)] for the HF potential. These peak positions are in the reasonable error limit of the maximum yield observed for the condensed phase plasmid DNA experiment (0.8 eV)[30]. The structure-less feature of the calculated fragmentation profile, here, further confirms the *impulse*[23] model behavior of the shape resonance process corroborating the time evolution plots of Fig. 3.

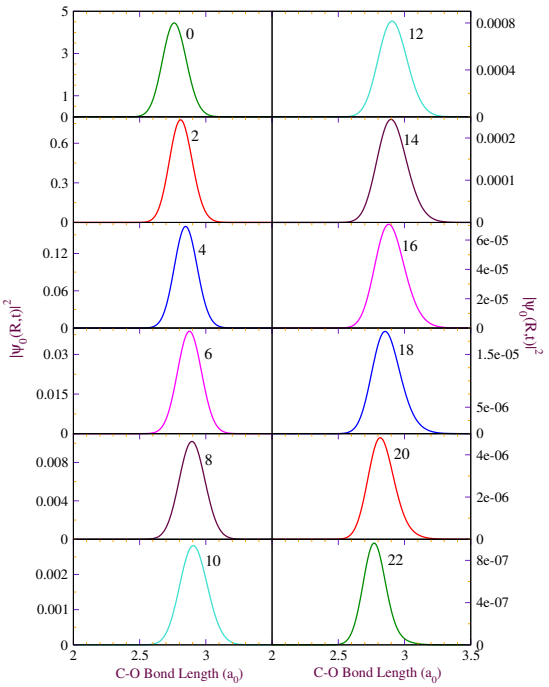

Fig. 3 Plots of wave packet propagation from time t = 0–22 fs for the ground state wave function ϕ_0(R) of the target 5′-dCMPH molecule under the effect of anionic Hamiltonian.

As mentioned earlier, the role of quantum mechanical tunneling phenomenon during the sugar phosphate 5′ C–O bond lesion may not be ruled out. Hence, we investigated the effect of tunneling during LEE induced SSB within this molecule for the first time and discussed in the following subsection 3.2.2.

3.2.2 SSB due to the C–O bond tunneling. The anionic PE curve [$E_{A^-}(R)$] of Figs. 2(a) and 2(b) has a barrier around 3.0 – 5.0 a_0 of the 5′ C–O bond length. We have divided $E_{A^-}(R)$ into three regions. Region 1 is the potential well where the LEE gets trapped forming the metastable state (or known as shape resonance state), Region 2 is the area under the barrier, and the repulsive asymptotic part of the potential designates as Region 3.

To proceed for the tunneling transmission coefficient calculation, we have to make use of either Eq. (7) or Eq. (8) which is solely depending upon the value of the constant K. However, since the barrier in $E_{A^-}(R)$ is not symmetric, therefore, it is difficult to find out the value of width parameter (a) which is the full width at the half maximum (FWHM) of the anionic PE curve. We have used a modeled hyperbolic cosine barrier

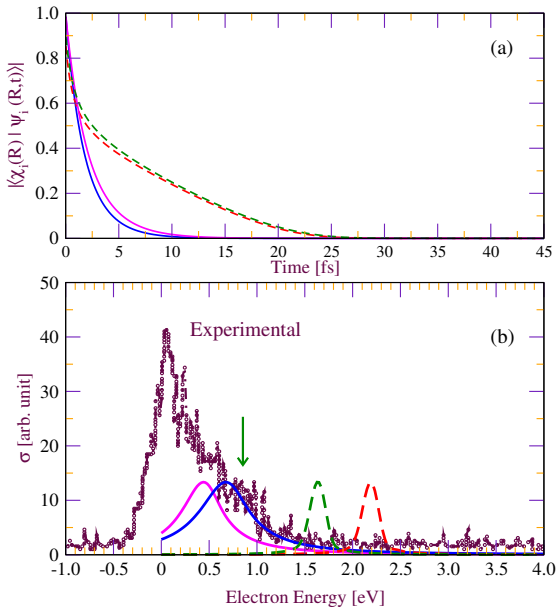

Fig. 4 (a) Auto correlation functions $|\langle\chi_i(R)|\psi_i(R,t)\rangle|$ calculated from wave packet propagation for 5′-dCMPH molecule at (i) HF/6-31+G(d) level (i=0, blue solid line and i=12, red dashed line), and (ii) MP2/6-31+G(d) level (i=0, magenta solid line and i=10, green dashed line) and, (b) comparison of corresponding $\sigma_{i\leftarrow i}$(E) for 5′-dCMPH molecule with the experimental profile[14] where the shoulder near 1 eV is labeled with an arrow.

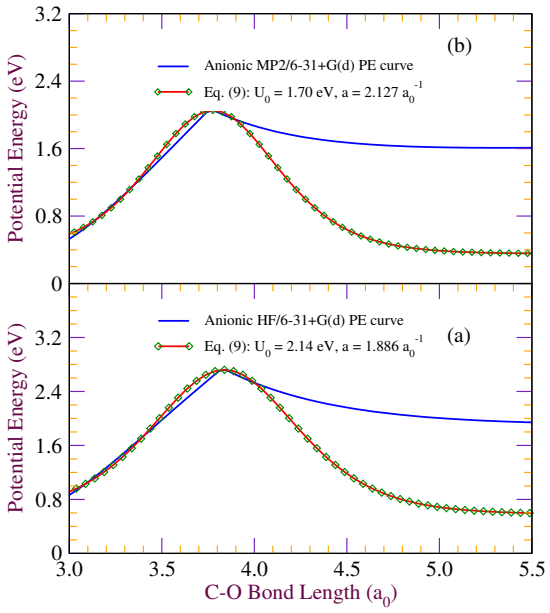

Fig. 5 (a) Comparison of analytical hyperbolic cosine curves fitted using Eq. (9) with the anionic PE curves of (a) Fig. 2(a) and (b) Fig. 2(b).

of the following form[29] to get the a value as:

$$U(R) = \frac{U_0}{\cosh^2(aR)} \tag{9}$$

where R corresponds to the 5′ C–O bond length of the anion. The analytical curve obtained using Eq. (9) is reasonably fitted well with the E_{A^-}(R), represented in Figs. 5(a) and 5(b). The value of K is found to be greater than one and thus, we have calculated the transmission coefficient (T) of the 5′ C–O bond tunneling from each of the fifteen bound vibrational levels ($\chi_{i=0-14}$) of MP2 anionic potential using Eq. (8). The best fitted values of "U_0" and "a" are taken as 1.70 eV and 2.13 $a_0{}^{-1}$ respectively for MP2 potential ("U_0"= 2.14 eV and "a"= 1.89 $a_0{}^{-1}$ for HF calculation). The variation of the tunneling probability against each of the anionic vibrational energies of HF and MP2 potentials are provided in Table 1 and Fig. S3†of the supporting information.

It can be seen from Table 1 and Fig. S3† that the probability of tunneling is completely suppressed from the lower vibrational levels [$\chi_{i=0-9}$(R) for MP2 and $\chi_{i=0-10}$(R) for HF anionic potentials]. However, at the χ_{10} state of MP2 potential (χ_{11} state of HF potential) a sudden jump in T is seen and that (T) becomes significant in the higher vibrational levels [$\chi_{i=11-14}$(R)] which may eventually contribute towards SSB. This characteristic tunneling behavior seen as "S-shaped" curve in Fig. S3† is already found in other investigations[29]. The surge in the transmission probabilities may be attributed to the increase in anionic vibrational energies from lower to higher vibrational states which allow a gradual flow of probability density towards the dissociative region of the E_{A^-}(R). Therefore, contribution of quantum mechanical tunneling of the 5′ C–O bond in SSB induced by LEE is prominent only from the metastable state formed in any one of the higher lying energy (> 1.5 eV) levels. Quantum mechanical tunneling of 5′ C–O bond from the upper lying states in *in vivo* DNA may be observed experimentally by achieving maximum population at these energy levels.

Further, to analyze the effect of quantum tunneling quantitatively from the higher vibrational levels ($\chi_{i=10-14}$) where T values are significant, we have chosen the χ_{10} state of E_{A^-}(R) of MP2 calculation (χ_{12} state of E_{A^-}(R) of HF calculation). The quantitative algorithm for wave packet propagation, auto correlation, and cross-section profile calculations have utilized the same as that mentioned in the earlier sub-section 3.2.1.

The wave packet motion of the initial state ψ_{10}(R, t=0) = ϕ_{10} (R) has been computed using Lanczos scheme[25] and provided a few of them in Fig. 6 (see Fig. S4† for HF potential). The time evolution plots of Fig. 6 reveals that the ten nodes of the initial wave function (t = 0 fs) reduces to four nodes within 5 fs. Subsequent profiles shows no nodes. Interestingly, there is a signature of shoulder and subsequent exponential decay of the wave function in the 20–25 fs plots. This feature is

Table 1 Transmission coefficient (T) calculated using Eq. (8)

Vibrational State (χ_i)	Vibrational Energy χ_i(E) [eV]		Transmission Coefficient (T)	
	HF	MP2	HF	MP2
0	0.65	0.42	1.95×10^{-29}	3.11×10^{-26}
1	0.79	0.55	8.59×10^{-26}	1.50×10^{-22}
2	0.93	0.68	1.65×10^{-22}	2.49×10^{-19}
3	1.07	0.81	1.66×10^{-19}	1.90×10^{-16}
4	1.20	0.93	9.84×10^{-17}	8.02×10^{-14}
5	1.33	1.05	3.76×10^{-14}	2.11×10^{-11}
6	1.46	1.18	9.94×10^{-12}	3.73×10^{-09}
7	1.59	1.30	1.89×10^{-09}	4.75×10^{-07}
8	1.72	1.42	2.71×10^{-07}	4.54×10^{-05}
9	1.84	1.54	3.01×10^{-05}	3.38×10^{-03}
10	1.97	1.65	2.66×10^{-03}	0.17
11	2.09	1.76	0.16	0.91
12	2.21	1.88	0.92	0.99
13	2.32	1.96	0.99	0.99
14	2.44	1.99	0.99	0.99
15	2.55	-	0.99	-
16	2.63	-	0.99	-
17	2.67	-	0.99	-

seen between $R_{C-O} \sim 3.2$–4.2 a_0 lies in the Region 2 ($R_{C-O} \sim$ 1.7–2.2 Å, tunneling region) of the Fig. 2(b) and may indicate quantum tunneling of the 5′ C–O bond from the χ_{10} state to the dissociative region. In addition, the metastable state at this vibrational state possesses a life-time of $\sim$ 60-65 fs which is much longer than that from the ground vibrational state ($\sim$ 18–20 fs). The larger spatial spread of the eigenfunction at χ_{10} may be the reason for the longer life-time. These findings are also supported by the calculated auto-correlation function $\langle\chi_{10}(R)|\psi_{10}(R,t)\rangle$ of Fig. 4(a) where the overlap is maximum at the initial time and reduces gradually to negligible values at t = 50 fs. Finally, the fragmentation profile calculated from the χ_{10} state exhibits a maximum at the 1.62 eV energy (2.19 eV for χ_{12} state of HF potential). The structure less feature of the spectrum in Fig. 4(b) once again enables us to infer the *impulse model*[23] classification of electron collision with this DNA fragment. The maximum of this spectrum has now been shifted to the higher energy region of the experimental maxima (0.83 eV in the condensed phase plasmid DNA investigation[30] and near 1 eV in the gas phase investigation of 5′-dCMP moiety[14]). This, thus, signifies pronounced 5′ C–O bond tunneling in the vibrational eigenstates of the 5′-dCMPH molecule above 1.5 eV energy. Our quantum dynamical predictions are reasonable with the available experimental observations.[14,30]

Apart from the quantitative approach discussed above, qualitative analysis from a series of generated molecular orbitals at MP2/6-31+G(d) accuracy level along the 5′ C–O potential energy curve shows the electron transfer pathway from the pyrimidine base to the back-bone phosphate P=O π^* orbital. The lowest unoccupied molecular orbital (LUMO) of the neutral 5′-dCMPH molecule at equilibrium C–O bond length [R_{C-O} = 2.75 a_0 (1.45 Å)] represents the π^* character located on cytosine base. Electron attachment to this molecular orbital does not alter it's π^* character on the base indicating a direct LEE attachment site in this nucleotide [Fig. 7(a)]. Singly occupied molecular orbital (SOMO) at the barrier height, R_{C-O} = 3.69 a_0 (1.95 Å) [Fig. 7(b)] shows the transfer of LEE to the C–O σ^* orbital. Once the LEE enters in to this repulsive state, it results in the rupture of the sugar-phosphate 5′ C–O bond producing highly stable phosphate anion and the pyrimidine nucleoside radical. This is evident from the SOMO generated at R_{C-O} = 5.67 a_0 (3.00 Å) as shown in Fig. 7(c) [See Fig. S5† for the similar trend in SOMOs generated at HF/6-31+G(d) accuracy level]. Thus, we state that the excess charge transfer originates from the base π^* orbital to the phosphate P=O π^* orbital through the valence 5′ C–O σ^* orbital. The large electron affinity ($\sim$ 5 eV) of the phosphate group[5] may facilitate the charge transfer process within a short period of time.[3]

Both the qualitative and quantitative analyses for LEE induced SSB in 5′-dCMPH molecule assures the role of *shape resonance* state present at the cytosine nucleobase.

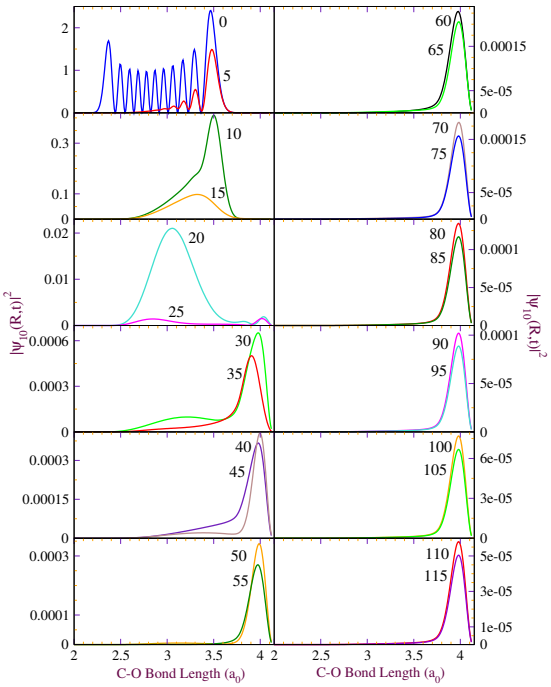

Fig. 6 Same as Fig. 3 except the target initial wave function is the eleventh vibrational state [ϕ_{10}(R)].

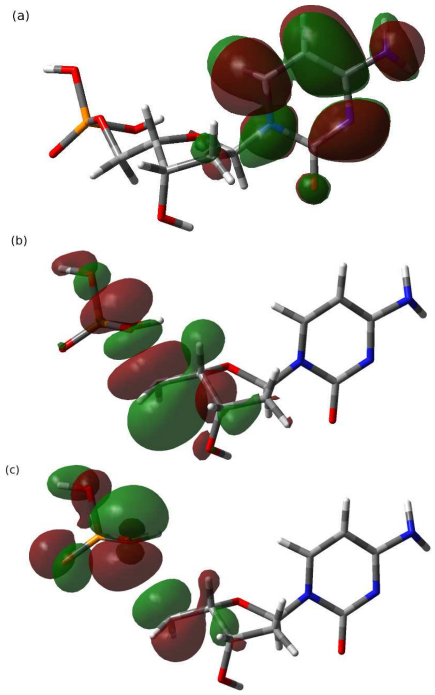

Fig. 7 Singly occupied molecular orbital (SOMO)s generated at the MP2/6-31+G(d) accuracy level for anionic 5′-dCMPH moiety for the 5′ C–O bond lengths of (a) 2.75 a_0 (1.45 Å), (b) 3.69 a_0 (1.95 Å), and (c) 5.67 a_0 (3.00 Å).

4 Concluding Remarks

We have provided the role of shape resonance state during LEE induced single strand breaks (SSBs) in a modeled DNA fragment 2′-deoxycytidine-5′-monophosphate (5′-dCMPH) in this investigation. The major outcome of our combined electronic structure and local complex potential based time dependent wave packet calculations are:

(a) LEE ($\sim$ 1 eV) can attach to the pyrimidine nucleobase cytosine leading to the formation of π^* shape resonance state.

(b) SSB can be occurred either from the ground vibrational levels (energy below 1.5 eV) of the metastable state or from the higher energy vibrational levels (above 1.5 eV) via quantum mechanical tunneling of the 5′ C–O bond.

(c) The metastable species possess a life-time of $\sim$ 18–20 fs at the ground vibrational level. The dissociation of 5′ C–O bond takes place even before it get time to execute single vibration.

(d) We could able to compare the calculated cross section spectrum in a reasonable manner with those of the available experimental [14,30] observations for the first time.

(e) In comparison with our previous investigations for both 3′ C–O and glycosidic N–C bonds dissociation in 3′-dCMPH molecule, [16–19] we suggest that both the 3′ and 5′ C–O bonds dissociation will be preferred over the glycosidic bond rupture since this metastable species possess slightly longer lifetime compared to that for the N–C bond scission.

The main features of the present investigation suggest the low energy electron attachment and subsequent decay of the metastable state occurs within a femtosecond time scale. In this ultrafast electron induced phenomenon, *shape resonance* state possess a major role. However, this is only a part (15 %) of the total SSB formation within this molecule. [14] The other major pathway (60 %) leading to 5′ C–O bond fragmentation is the initial localization of LEE at the phosphate center of the nucleotide. [14] The likely mechanism of charge transfer for this pathway has to be remain investigated theoretically. Also, one has to consider the role of vibrational Feshbach resonance (VFR) during LEE induced SSB within this molecule. We are currently working along this line. In addition, we also believe that higher level correlated methods (for e.g., coupled cluster) with larger basis set expansions may improve the description of the dynamics in terms of the resonance energy position and the barrier height determination. Finally, we hope our findings offer a threshold for further investigations in other nucleotide units or DNA fragments for LEE induced damage and the LCP-TDWP approach can help to bring about the characteristics features of the electron scattering off DNA and DNA fragments.

Acknowledgements

R.B acknowledges the financial support from Ministry of Human Resource Development (MHRD), Government of India. We are thankful to Prof. Ashish K. Gupta (IIT Guwahati) for providing the computational facilities. We are also grateful to IIT Guwahati for providing infrastructure facilities.

References

1 L. Sanche, *Eur. Phys. J. D*, 2005, **35**, 367–390.

2 I. Baccarelli, I. Bald, F. A. Gianturco, E. Illenberger and J. Kopyra, *Phys. Rep.*, 2011, **508**, 1–44 and references therein.

3 J. Gu, J. Leszczynski and H. F. Schaefer III, *Chem. Rev.*, 2012, **112**, 5603–5640.

4 B. Boudaïffa, P. Cloutier, D. Hunting, M. A. Huels and L. Sanche, *Science*, 2000, **287**, 1658–1660.

5 J. Simons, *Acc. Chem. Res.*, 2006, **39**, 772–779 and references therein.

6 K. Aflatooni, G. A. Gallup and P. D. Burrow, *J. Phys. Chem. A*, 1998, **102**, 6205–6207.

7 S. Ptasinska, S. Denifl, P. Scheier and T. D. Mark, *J. Chem. Phys.*, 2004, **120**, 8505–8511.

8 X. Li, M. D. Sevilla and L. Sanche, *J. Am. Chem. Soc.*, 2003, **125**, 13668–13669.

9 A. M. Scheer, K. Aflatooni, G. A. Gallup and P. D. Burrow, *Phys. Rev. Lett.*, 2004, **92**, 068102-1–068102-4.

10 L. Sanche, *Chem. Phys. Lett.*, 2009, **474**, 1–6.

11 S. M. Pimblott and J. A. LaVerne, *Radiat. Phys. Chem.*, 2007, **76**, 1244–1247.

12 E. Alizadeh and L. Sanche, *Chem. Rev.*, 2012, **112**, 5578–5602 and references therein.

13 M. A. Huels, B. Boudaïffa, P. Cloutier, D. Hunting and L. Sanche, *J. Am. Chem. Soc.*, 2003, **125**, 4467–4477.

14 J. Kopyra, *Phys. Chem. Chem. Phys.*, 2012, **14**, 8287–8289.

15 X. Bao, J. Wang, J. Gu and J. Leszczynski, *Proc. Natl. Acad. Sci. U.S.A.*, 2006, **103**, 5658–5663.

16 R. Bhaskaran and M. Sarma, *J. Chem. Phys*, 2014, **141**, 104309-1–104309-9.

17 R. Bhaskaran and M. Sarma, *J. Chem. Phys*, 2013, **139**, 045103-1–045103-9.

18 S. Bhowmick, Renjith B, M. K. Mishra, and M. Sarma, *J. Chem. Phys*, 2012, **137**, 064310-1–064310-8.

19 Renjith B, S. Bhowmick, M. K. Mishra, and M. Sarma, *J. Phys. Chem. A*, 2011, **115**, 13753–13758.

20 H. Chen, P. Yang, H. Chen, C. Kao and L. Liao, *J. Phys. Chem. B*, 2014, **118**, 11137–11144.

21 M. J. Frisch, G. W. Trucks, H. B. Schlegel, G. E. Scuseria, M. A. Robb, J. R. Cheeseman, G. Scalmani, V. Barone, B. Mennucci, G. A. Petersson, H. Nakatsuji, M. Caricato, X. Li, H. P. Hratchian, A. F. Izmaylov, J. Bloino, G. Zheng, J. L. Sonnenberg, M. Hada, M. Ehara, K. Toyota, R. Fukuda, J. Hasegawa, M. Ishida, T. Nakajima, Y. Honda, O. Kitao, H. Nakai, T. Vreven, J. A. Montgomery, Jr., J. E. Peralta, F. Ogliaro, M. Bearpark, J. J. Heyd, E. Brothers, K. N. Kudin, V. N. Staroverov, T. Keith, R. Kobayashi, J. Normand, K. Raghavachari, A. Rendell, J. C. Burant, S. S. Iyengar, J. Tomasi, M. Cossi, N. Rega, J. M. Millam, M. Klene, J. E. Knox, J. B. Cross, V. Bakken, C. Adamo, J. Jaramillo, R. Gomperts, R. E. Stratmann, O. Yazyev, A. J. Austin, R. Cammi, C. Pomelli, J. W. Ochterski, R. L. Martin, K. Morokuma, V. G. Zakrzewski, G. A. Voth, P. Salvador, J. J. Dannenberg, S. Dapprich, A. D. Daniels, O. Farkas, J. B. Foresman, J. V. Ortiz, J. Cioslowski, and D. J. Fox, *Gaussian 09*, Revision D.01, Gaussian,Inc. Wallingford, CT, 2013.

22 L. Dubé and A. Herzenberg, *Phys. Rev. A*, 1979, **20**, 194–213.

23 J. N. Bardsley and J. M. Wadehra, *Phys. Rev. A*, 1979, **20**, 1398–1405.

24 C. C. Marston and G. G. Balint-Kurti, *J. Chem. Phys.*, 1989, **91**, 3571–3576.

25 C. Leforestier, R. H. Bisseling, C. Cerjan, M. D. Feit, R. Friesner, A. Guldberg, A. Hammerich, G. Jolicard, W. Karrlein, H.-D. Meyer, N. Lipkin, O. Roncero and R. Kosloff, *J. Comput. Phys.*, 1991, **94**, 59–80.

26 D. Kosloff and R. Kosloff, *J. Comput. Phys.*, 1983, **52**, 35–53.

27 J. Zhang, D. G. Imre and J. H. Frederick, *J. Phys. Chem.*, 1989, **93**, 1840–1851.

28 L. D. Landau and E. M. Lifshitz, *Quantum Mechanics, 3rd ed.*, Pergamon Press, Oxford, U.K., 1977.

29 R. Marom, C. Levi, T. Weiss, S. Rosenwaks, Y. Zeiri, R. Kosloff and I. Bar, *J. Phys. Chem. A*, 2010, **114**, 9623–9627.

30 F. Martin, P. D. Burrow, Z. Cai, P. Cloutier, D. Hunting and L. Sanche, *Phys. Rev. Lett.*, 2004, **93**, 068101-1–068101-4.